Int. J. Electrochem. Sci., 10 **(2015)** 9556 - 9570

International Journal of
ELECTROCHEMICAL
SCIENCE
www.electrochemsci.org

Study on the Properties of Fuel Cell 304 Stainless Steel Bipolar Plates with Flow Channels Milled Using Different Methods

Te Yuan Chiang[1], *Ay Su*[1,*]

Department of Mechanical Engineering, Yuan Ze University, Taiwan, ROC
[*]E-mail: teyuanchiang@gmail.com

Received: 24 June 2015 / *Accepted:* 7 September 2015 / *Published:* 30 September 2015

Various materials are currently used as bipolar plate flow channel substrates in proton exchange membrane fuel cells (PEMFCs): stainless steel, carbon steel, copper, aluminium, graphite, etc. Stainless steel has the best corrosion resistance among these materials but is more difficult to machine. Stainless steel exhibits the following characteristics during cutting: severe processing-induced hardening, a large cutting resistance, a high cutting temperature and chips that do not break easily and are prone to adhesion and tool wear. In the experiments reported here, SUS304 stainless steel was used as a substrate to explore the impact of using different methods, rotation rates, feed rates and cooling methods to mill flow channels for the subsequent anti-corrosion treatment of the specimens. After milling, the flow channels and the specimens were plated with chrome-carbon (Cr-C) to improve the corrosion resistance and conductivity of the substrates. After plating, the specimens that were fabricated using the high-speed milling machine performed better in all aspects and exhibited overall better corrosion resistance and electrical properties, as measured by potentiodynamic and potentiostatic polarization tests, than the other specimens. The results of our study can serve as a reference for the processing of PEMFC bipolar plates.

Keywords: bipolar plates, flow channel milling, chrome-carbon plating

1. INTRODUCTION

Significant resources have been expended worldwide in research on alternative energy sources with high efficiencies and low pollution. Among these alternatives, fuel cells with high energy conversion efficiencies have become the focus of research for future green energy applications. In particular, proton exchange membrane fuel cells (PEMFCs) have low operating temperatures and high conversion efficiencies [1] and are thus suitable for mobile power applications. However, current development of PEMFCs is facing a bottleneck: the cost for manufacturing and assembling bipolar plates is approximately 45 to 30% of the overall cost of the cell [2]. That is, high material costs have

become the most important factor preventing PEMFC commercialisation. Thus, the key to improving fuel cell (array) performance and developing a more economical mass production technology is the availability of bipolar plates with higher performance and lower manufacturing costs [3].

The materials that are used in conventional bipolar plates are primarily graphite sheets, which are desirable electrode materials because of their low resistance and anti-corrosive properties. Graphite can produce a stable battery output power and is chemically stable. However, graphite is a brittle material with several corresponding drawbacks, including processing challenges and poor mechanical properties. In addition, it is difficult to fabricate gas flow channels in thin graphite bipolar plates by machining; thus, bipolar plates cannot be thinned to reduce costs or improve power. A metal bipolar plate has good electrical conductivity, is light weight, has excellent mechanical properties and can be easily moulded. Thus, metal bipolar plates have become the focus of research worldwide. Stainless steel, aluminium alloys and titanium alloys are currently commonly used materials for bipolar plates.

The conventional application of stainless steel has several drawbacks in stainless steel cutting. 1. Severe processing-induced hardening can occur: the steel structure can be be damaged and dispersedly distributed to form hardened layers under the action of stress during cutting. 2. A high cutting force is required because stainless steel exhibits large plastic deformation during cutting. Meanwhile, severe hardening during stainless steel processing and the high thermal density of stainless steel can cause a further increase in the cutting resistance and create difficulties in chip breaking. 3 A high cutting temperature is required: more heat is generated during cutting if there is large plastic deformation and large friction against the tool. Furthermore, most of the heat becomes concentrated in the cutting zone and at the interface that is in contact with the cutting tip because of the low thermal conductivity of stainless steel (which is approximately 1/2-1/4 of the thermal conductivity of No. 45 carbon steel) and poor heat dissipation. Under the same conditions, the cutting temperature of 1Cr18Ni9Ti is approximately 200 °C higher than that of No. 45 carbon steel. 4. The swarf is hard to break but easy to adhere to. The high ductility and plasticity of stainless steels results in the production of continuous long swarves during machining that not only affect the operation but also crush the machined surface. Stainless steels have a high affinity for other metals under high temperatures and pressures and are thus prone to adhere to other metals, which results in built-up edges (BUEs) and increases tool wear and tear that damages the machined surface. 5 Tool wear: the affinity of stainless steel for metals can cause adhesion and diffusion between tools and swarves during cutting, resulting in tool wear from adhesion and diffusion.

The traditional milling method of computer numerical control (CNC) to cut stainless steel results in a finished product with poor mechanical properties and flow channels with high surface roughness. The high surface roughness of the flow channels increases the surface area, resulting in incomplete plating and reduced conductivity of the bipolar plates. Therefore, studies are currently being conducted on using high-speed milling machines to cut bipolar plates. The metal bipolar plates in battery systems are affected by the environment (i.e., the presence of F^-, SO_4^{2-}, SO_3^{2-}, HSO^-, HSO_3^-, CO_3^{2-} and HCO_3^- anions) [4]; thus, the surface can easily oxidise to form a passivation film, which increases the contact resistance and reduces the battery performance. In addition, electrochemical corrosion can occur on metals in a solution environment, leading to the poisoning of the ion exchange

membrane of the cell [5, 6]. Thus, the metal substrate needs to be coated with an anti-corrosion film. Numerous studies have been conducted on the anticorrosion treatment of metal bipolar plates [7-12], and considerable progress has been made on chromising through low-temperature pack cementation [13-19]. However, anti-corrosion coatings that perform well on flat metal substrates usually perform poorly on substrates with flow channels. Thus, it is important to explore the effect of channel processing on an anti-corrosion treatment [20-25].

The objective of this study was to explore the corrosion resistance of chromised nickel (Ni)-plated SUS304 stainless steel with flow channels that were milled at different speeds by different methods to improve the performance and durability of fuel cell bipolar plates. Chromate was coated onto the stainless steel surface using non-vacuum thermal deposition. Flow channels were machined into the specimen with the feed rate as the major processing parameter. The corrosion resistance of the machined substrate surface was investigated to determine the effect of different processing conditions on the properties of the coating surface. Thus, processing conditions could be selected for the economical mass production of light and thin plates or bipolar plate miniaturisation.

2. EXPERIMENTAL

2.1. Specimen preparation

Table 1 provides the composition of SUS304 stainless steel that was used as the bipolar plate substrate. The specimen was prepared by first cutting the steel plate into specimens with dimensions of 50 mm × 50 mm × 2 mm, followed by soaking in acetone or ethanol and sonication to remove surface grease.

The flow channels were milled in the machining centre (MC) using a Ø 1.0-mm round cutter. The spindle rotation was fixed at 8000 rpm, and the feed rates were set in the range of 100-200 mm/min with a 50 mm/min interval. The milling depth was 1 mm: the milling process was completed in 6 separate cuttings and cooled using soluble oil. The second cutting process consisted of fine milling to form flow channels. Different processing parameters were used to investigate their effects on the anti-corrosion surface treatment and to simulate the plating conditions for actual channels.

Table 1. Chemical composition of the SUS 304 steel.

Elements	C	P	Mn	S	Fe
wt(%)	0.45	0.04	0.7	0.05	Balance

2.2. Chrome-carbon plating

The specimens (SS304 stainless steel substrate with flow channels) that were subjected to chrome (Cr)-carbon (C) plating were sequentially degreased and pre-treated with basic and acid washes. The specimens were degreased by soaking in acetone for 2 minutes at room temperature,

followed by washing with pure water. The specimens were then washed with NaOH (30 g/L) at 25 °C for 60 seconds, followed by washing with pure water. Finally, the specimens were washed in 10% hydrochloric acid at room temperature for one minute, followed by a pure water wash.

The major salt in the Cr-C plating bath solution was Cr chloride, and the solution consisted of $CrCl_3 \cdot 6H_2O$ (0.3 M), a chelating carboxylic acid (2 M), a conductive salt (Ammonium sulfate, $(NH_4)_2SO_4$, 1 M), a buffer (Potassium hexafluorozirconate, KZrF6, 0.7 M) and additives (Potassium bromide, KBr, 0.03 M). The chemicals were added to the water in the aforementioned order and stirred to dissolve before adding the next component an hour later. Once all the chemicals had been added, the solution was stirred for 1 hour. After the chelation of the plating bath solution was complete, plating was initiated. The operating parameters were a plating current density of 10 A/dm^2, a plating time of 10 min, a temperature of 25 °C and a pH of 4.

The plating was conducted after the pretreatment. The specimens were plated in the plating solution, followed by a deionised water rinse to remove any residual plating solution on the surface of the specimens. The specimens were then immediately blown dry using an air compressor and set aside for subsequent measurement.

2.3. Corrosion test

The corrosion resistance was measured using a potentiodynamic polarization test. The specimen was placed in a simulated PEMFC environment (0.5 M H_2SO_4, room temperature), and the potentiodynamic polarisation test was conducted on the specimen using a potentiostat. A calomel electrode was used as the reference electrode (REF) with a standard reduction potential of 0.244 V with respect to the standard hydrogen electrode (SHE). The working electrode (WE) was connected to the specimen. All experiments were conducted in an Autolab PGSTAT30 potentiostat/galvanostat controlled by the GPES (General Purpose Electrochemical System) software. The linear polarization curves were measured in the potential range between −1 V and 0.8 V referred to open circuit potential, with a scanning rate of 0.5 mV s^{-1}. The voltage and current during the experiment were recorded and used to plot polarisation curves. A potentiostatic test was conducted in a simulated fuel cell cathode environment. When potentiostatic tests were performed, the 0.6V (vs. SCE) potential with air purging was applied to simulate the cathodic environment in a 0.5 M H_2SO_4 solution at 80 ◦C for 1 h.

2.4. Contact resistance

Red copper plates were used to sandwich two gas diffusion layers (GDL) and a specimen that was previously fabricated, which were then connected to an ohmmeter. For measuring the contact resistance, two pieces of carbon paper were sandwiched between the specimen and two copper plates. During the tests, a constant electrical current was provided through the copper plates, and the variation in the total voltage was recorded with respect to the compaction force that was steadily increased from 0 to 200 Ncm^{-2} and recorded with every 9.8 Ncm^{-2}. The contact resistance had to be reduced because a high contact resistance would have caused most of the energy to be converted into heat and reduced

the power. Previous studies have shown that applying different pressures on graphite bipolar plates and gas diffusion layers can cause changes in the contact resistance [26]. At low pressures, the contact resistance decreases with increasing pressure; however, as the pressure increases, the contact resistance no longer decreases and instead the diffusion path for mass transfer from the flow channel to the catalyst layer shrinks, effectively inhibiting any increase in the power. The conductivity of the specimen made was assessed by measuring the contact resistance of the specimen.

3. RESULTS AND DISCUSSION

3.1. Coating microstructure

Flow channels with different inner surface morphologies were obtained by changing the cutting and feed rates during the flow channel machining. The specimen code is given in Table 2. Examination of the surface morphology showed that different feed rates caused different traces. Fig. 1 shows scanning electron microscopy (SEM) pictures of the surface morphology inside the flow channels in Ni-plated metal bipolar plates that were milled at different feed rates. The cutting traces inside the flow channels were significantly reduced by fine milling. Fig. 2 is an SEM image of a portion of the flow channel cross-section for Ni-plated bipolar plates. The cross-sectional view shows that the Ni coating on the interior of the flow channel became thinner as the distance from the anode increased. The coating thickness on the flat surface was approximately 12 μm, the coating thickness on the side of the channel was approximately 10 μm, and the coating thickness at the bottom of the channel was approximately 6 μm. Fig. 3 shows SEM images of the surface morphology of the pack cementation-treated flow channels in the metal bipolar plates that were milled at different feed rates. The differences caused by the pack cementation temperature can be seen in the cutting traces inside the flow channel that were distributed on the side and at the bottom of flow channels, depending on the feed rate (fast, slow and fast). The primary reason for this result is that the high temperature caused by the continuous moving and scratching of the cutter on the work surface caused the metals to adhere and then fall off, resulting in defects. When cutting was performed at an ultra-high rotation and a relatively low feed rate, the cutter generated less tear and stress on the materials when traveling, which was not likely to cause defects on either side of the flow channel arc. These cutting traces were nearly completely eliminated by fine milling, possibly because of the reduced local hardening and plastic deformation that were generated during the processing and the reduced impact on the coating surface morphology by the thermal treatment in pack cementation. In particular, using a suitable feed rate during high-speed milling greatly reduced the cutting trace inside the flow channels of specimen 304mm100-Ni30-Cr(800-2) after Ni plating, pack cementation and the deposition of the Cr-C coating. Fig. 4 is an SEM picture of the flow channel cross-section in the metal bipolar plates after pack cementation. The cross-section morphology at this stage shows that the Cr-C coating was 2.5 μm thick on the flat surface and 1.5 μm thick at the bottom of the flow channels. The second layer was a Ni-iron (Fe) miscible layer. The high miscibility between Ni and Fe at high temperatures caused the Fe atoms in the pack cementation-treated substrate to diffuse outward and form a thick miscible layer with Ni plating.

Table 2. Specimen names and the corresponding conditions

Specimen name	feed rate	activated[a]	condition[b]
304-Ni30-Cr(800-2)	—	Ni-plated 30min	800˚C, 2hour
304-1mm(50a)-Ni30-Cr(800-2)	50 mm/min	Ni-plated 30min	800˚C, 2hour
304-1mm(75a)-Ni30-Cr(800-2)	75 mm/min	Ni-plated 30min	800˚C, 2hour
304-1mm(100a)-Ni30-Cr(800-2)	100 mm/min	Ni-plated 30min	800˚C, 2hour
304-1mm(125a)-Ni30-Cr(800-2)	125 mm/min	Ni-plated 30min	800˚C, 2hour
304-1mm(150a)-Ni30-Cr(800-2)	150mm/min	Ni-plated 30min	800˚C, 2hour
304-1mm(175a)-Ni30-Cr(800-2)	175 mm/min	Ni-plated 30min	800˚C, 2hour
304-1mm(200a)-Ni30-Cr(800-2)	200 mm/min	Ni-plated 30min	—

a Activation treatment

b Chromisation temperature and duration

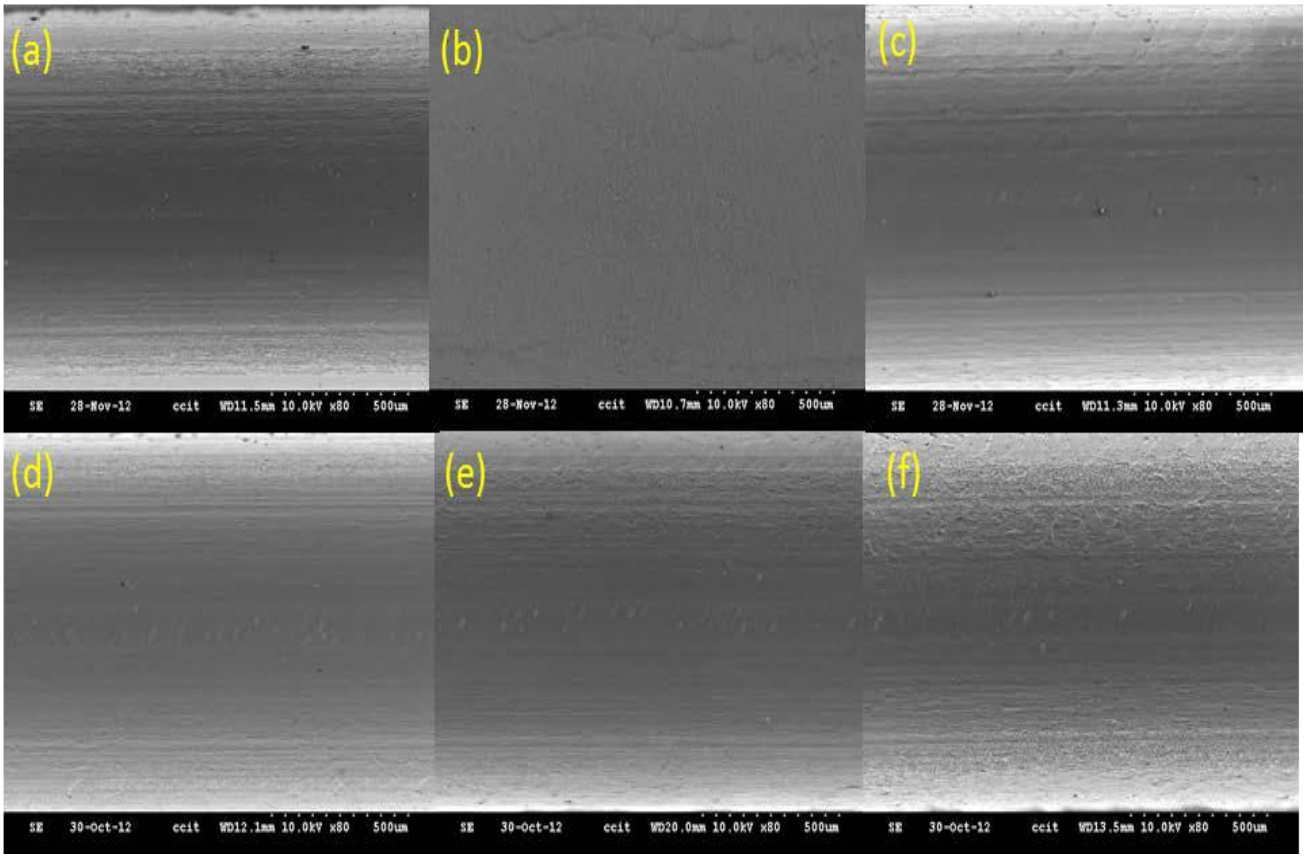

Figure 1. Morphologies of nickel plated specimen at channel under different feed rate of (a) 50 mm/min; (b)75 mm/min; (c)100 mm/min; (d)125 mm/min; (e)150 mm/min; (f) 175 mm/min.

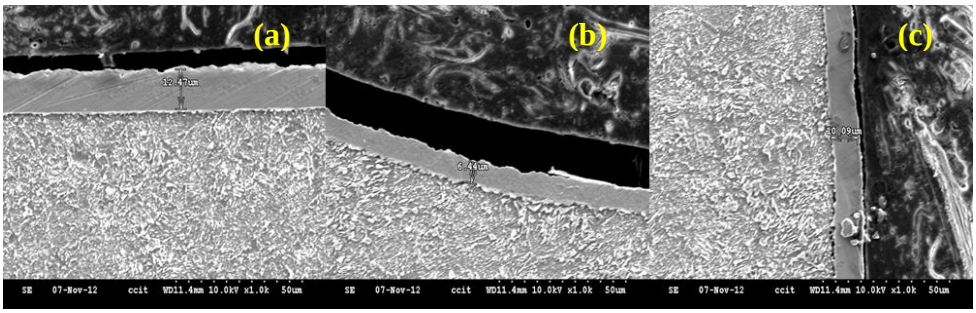

Figure 2. Cross-sectional SEM images of nickel plated specimen at (a)surface; (b)bottom of channel; (c)side well of channel.

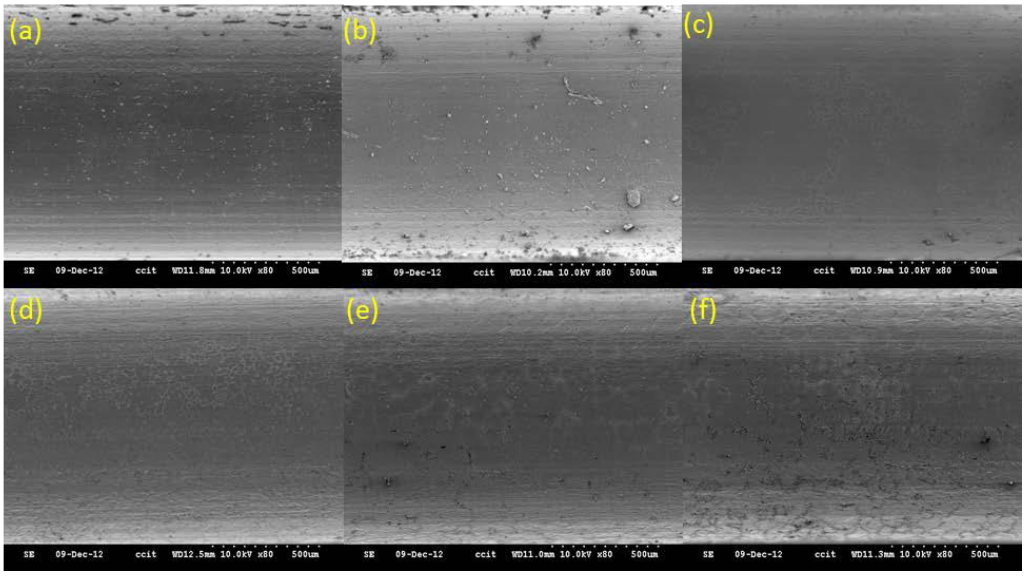

Figure 3. Morphologies of pack cementation finished specimen at channel under different feed rate of (a) 50 mm/min; (b)75 mm/min; (c)100 mm/min; (d)125 mm/min; (e)150 mm/min; (f) 175 mm/min.

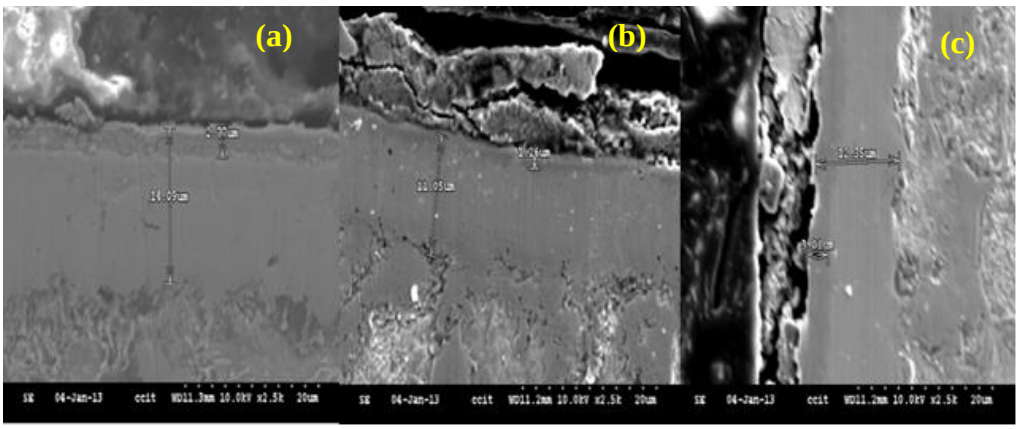

Figure 4. Cross-sectional SEM images of pack cementation finished specimen at (a)surface; (b)bottom of channel; (c)side well of channel.

3.2. Elemental analysis of chromised specimen

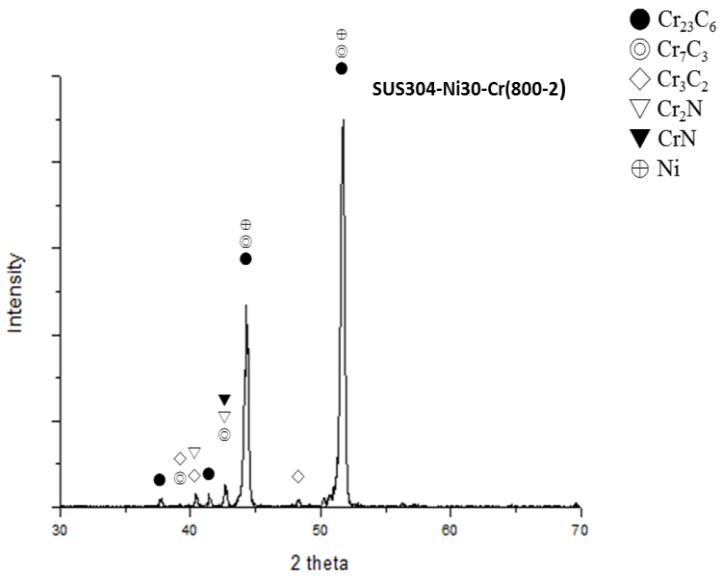

Figure 5. XRD pattern of pack cementation finished specimen.

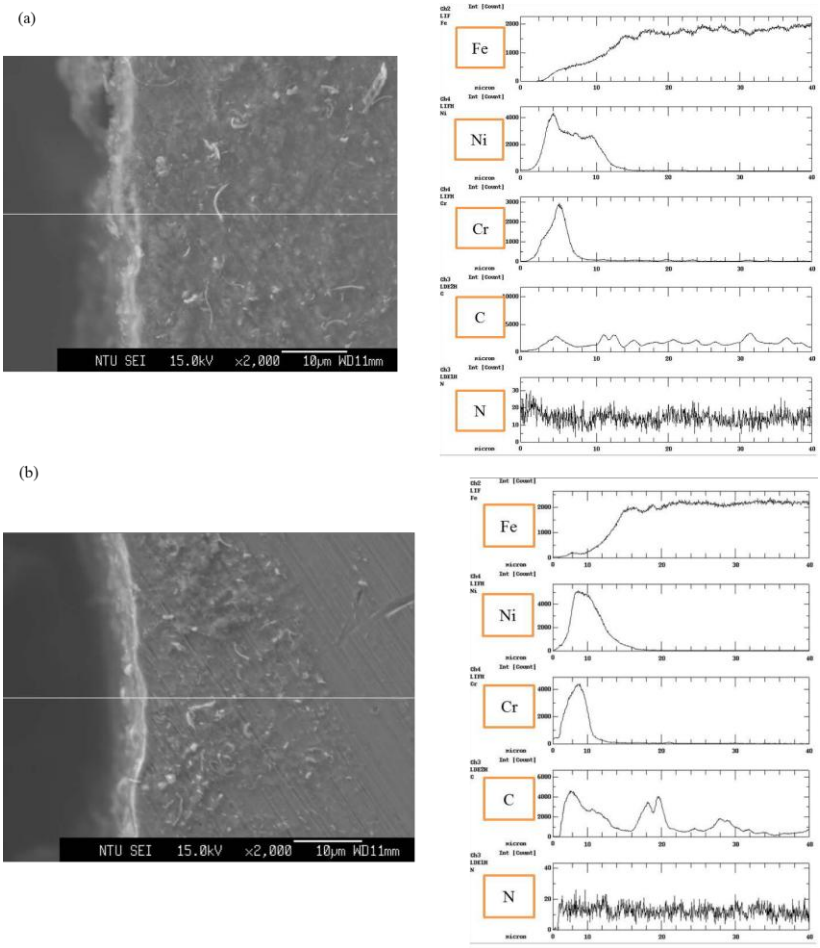

Figure 6. EPMA line-scans of Fe, Ni, Cr, C, and N of pack cementation finished specimen. (a)surface; (b)bottom of channel.

Fig. 5 shows the XRD curve of the metal bipolar plates after pack cementation. The figure shows that the Cr-C coating primarily consisted of Cr-C compounds and a small quantity of Cr nitrate. During pack cementation, the high temperature provided sufficient energy for the chrome atoms to diffuse from the Cr solid into the plated Ni layer and react with the carbon atom in the substrate to form Cr carbonates, whereas nitrides were primarily generated by the high-temperature decomposition of ammonium chloride. Fig. 6 is a cross-sectional element line scan of the metal bipolar plate surface and the bottom of the flow channels after pack cementation. The figure shows that there was a very small quantity of Fe in the Cr-C coating, indicating that the Ni plating played the dominant role in protecting the Cr-C coating. The Cr was miscible with the electroplated Ni during thermal diffusion; thus, on the surface of the plating layer, a solid solution formed between the Ni, Cr and C from the substrate, in the bottom of the plating layer and between the Ni in the bottom of the plating layer and the Fe from the substrate.

3.3. Electrochemical test

3.3.1 Potentiodynamic polarization test

The specimens (SUS304 substrate) with flow channels that were milled at different rotations and feed rates underwent the same pack cementation chromising treatment, followed by potentiodynamic polarization tests in a 0.5 M H_2SO_4 solution at room temperature. Fig. 7 shows the potentiodynamic polarization curve for the Ni-plated specimens that were milled at different feed rates. The figure shows that precision milling reduced the cutting traces and chips inside the flow channel, resulting in a smoother inner channel surface. Thus, Ni was evenly coated onto the flow channel surface, which enhanced the corrosion resistance. The nickel layer played a role to protect the SUS304 stainless steel substrate. Fig. 8 shows the potentiodynamic polarization curves for the pack cementation-treated specimens that were milled using different processing parameters. It revealed that the specimens milled at 50, 75 and 175 mm/min had poor corrosion resistance, it can be attributed to the slow or overly fast feed rates would remain deep cutting traces and a rough surface inside the flow channel. Thus, the surface was not completely covered even after pack cementation, and the Ni plating could not completely protect the substrate, which reduced the corrosion resistance. The trend in the corrosion current (I_{corr}), Tafel slope βa and cathodic Tafel slope βc for the specimens are listed in Table 3 also supported the observation of the morphology of the pack cementation-treated flow channels (see Fig. 3). All these polarization curves have similar shapes in anodic and cathodic branches. The anodic and cathodic Tafel constants do not obviously change for samples, which show that the similar mechanism for corrosion reaction. The results of the potentiodynamic polarization test showed that these relatively deep cutting traces could easily cause passivation of the Cr-C coating.

The enhanced processing parameters and subsequently smaller cutting traces inside the flow channel resulted in an even Ni plating inside the flow channel of specimen 304-1mm100-Ni30-Cr(800-2) that was milled at a feed rate of 100 mm/min, and the Cr coating also completely covered the Ni plating after pack cementation. Thus, the Ni plating protected the substrate and prevented Fe from diffusing into the Cr-C layer, which reduced the passivation. The values of the corrosion current (I_{corr}),

corrosion potential, Tafel slope βa and cathodic Tafel slope βc for the specimens after pack cementation are given in Table 4. The results showed the substrates milled at the feed rate range between 100 and 150 mm/min and then completed a surface treatment process would obtain better protective behaviour due to a smoother surface on the flow channels. The protective efficacy of specimens from substrates formed completely covered the Ni plating and pack cementation indeed better than that of only covered the Ni plating in this work and previous study [27, 28].

Table 3. The corrosion parameters of specimens after nickel plated

Specimens	β a (V/ decade)	β c (V/ decade)	I_{corr} (A/cm^2)	E_{corr} (V)
304-1mm(50a)-Ni30	208.51	-374.45	9.72×10^{-5}	-0.295
304-1mm(75a)-Ni30	324.78	-417.65	3.92×10^{-5}	-0.290
304-1mm(100a)-Ni30	297.47	-449.74	3.72×10^{-5}	-0.295
304-1mm(125a)-Ni30	268.74	-386.67	2.58×10^{-5}	-0.312
304-1mm(150a)-Ni30	247.57	-403.86	2.35×10^{-5}	-0.300
304-1mm(175a)-Ni30	228.54	-394.66	2.27×10^{-5}	-0.304
304-1mm(200a)-Ni30	339.48	-434.37	8.08×10^{-5}	-0.355

Table 4. The corrosion parameters of specimens after pack cementation.

Specimens	β a (V/ decade)	β c (V/ decade)	I_{corr} (A/cm^2)	E_{corr} (V)
304-1mm(50a)-Ni30-Cr(800-2)	126.54	-216.64	2.55×10-6	-0.253
304-1mm(75a)-Ni30-Cr(800-2)	104.38	-198.62	1.41×10-6	-0.134
304-1mm(100a)-Ni30-Cr(800-2)	328.76	-405.73	6.93×10-7	-0.167
304-1mm(125a)-Ni30-Cr(800-2)	419.38	-578.52	9.57×10-7	-0.088
304-1mm(150a)-Ni30-Cr(800-2)	461.73	-612.74	9.87×10-7	-0.108
304-1mm(175a)-Ni30-Cr(800-2)	196.48	-286.41	3.71×10-6	-0.156

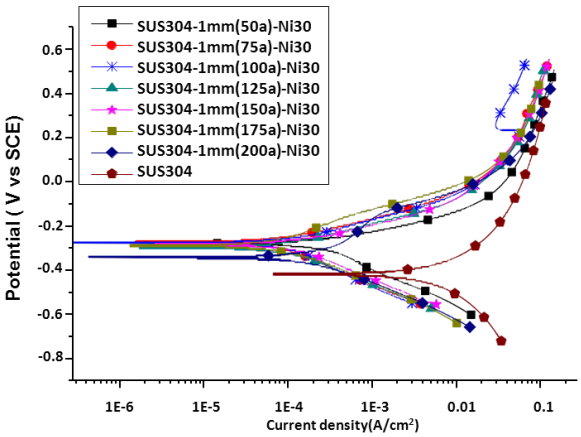

Figure 7. Polarization curves of bare and nickel plated specimen with differential feed rate channel

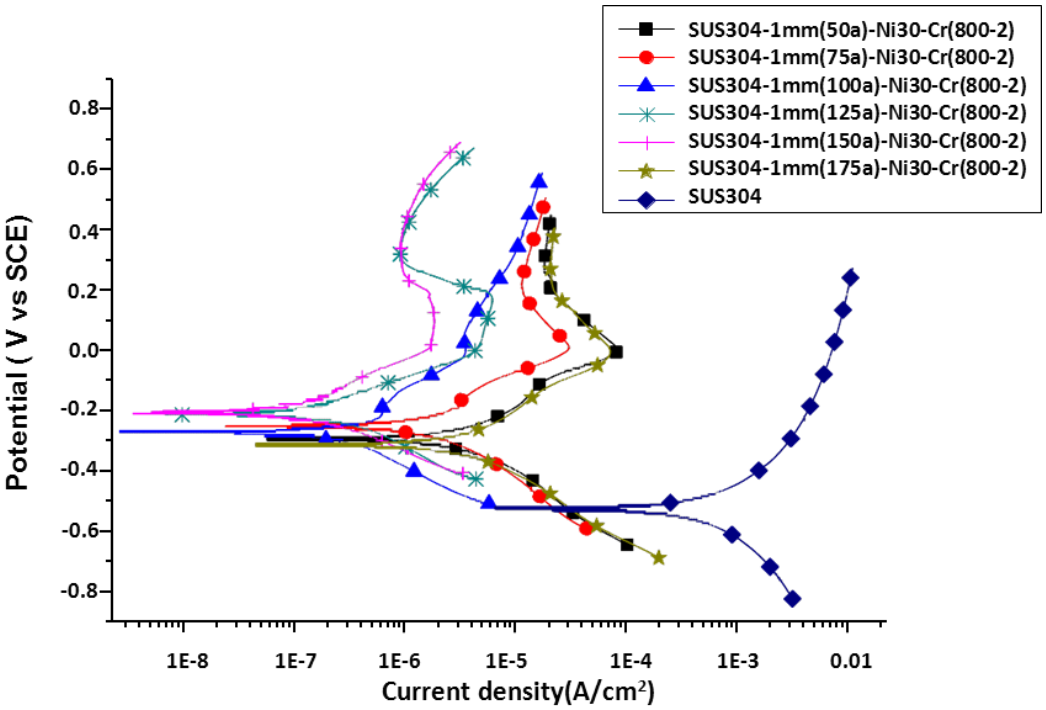

Figure 8. Polarization curves of bare and pack cementation finished specimen with differential feed rate channel.

3.3.2 Potentiostatic polarization test

In general, the fuel cell systems must undergo potentiostatic measurements. The cathode of an operating fuel cell typically undergoes anodic corrosion. In this study, the simulated cathode potential was set to 0.6 V; the ambient temperature was set to 80 °C, and the operating time was 1 h. Fig. 9 presented the current density recorded as a function of time for the chromised specimens that were milled at different feed rates with that of the chromised specimens without flow channels. The curves showed that the initial current density increased in the following order: SUS304-1mm75-Ni30-Cr(800-2) > SUS304-1mm125-Ni30-Cr(800-2) > SUS304-1mm150-Ni30-Cr(800-2) > SUS304-1mm100-Ni30-Cr(800-2) > SUS304-Ni30-Cr(800-2). As mentioned above, the SEM results showed that there was a considerable quantity of chips on the bottom of specimen SUS304-1mm75-Ni30-Cr(800-2); therefore, the plating could not withstand the harsh environment of the high voltage (0.6 V) and the high temperature (80 °C) with air purging. Thus, the current density was very initially large and increased with time.

The initial current density of SUS304-1mm125-Ni30-Cr(800-2) was 9.2E-5 A/cm2, and the corresponding plating was very stable during the 1-hour potentiostatic polarization test. However, the current density did not meet the U.S. Department of Energy's (DOE) 2015 standard of 1E-6 A/cm^2. The initial current of specimen SUS304-1mm150-Ni30-Cr(800-2) was 4.3E-5 A/cm^2, which began to increase slightly from 600 seconds onwards until the end of the test. The initial current density of specimen SUS304-1mm100-Ni30-Cr(800-2) was 2.4E-5 A/cm^2 and remained constant until the end of the test; the plating for this specimen was more stable than that of SUS304-1mm150-Ni30-Cr(800-2),

and an increase in the current density was not observed. Fig. 10 is an enlarged image of the local areas of the chromised flow channel specimens that were milled at different feed rates, which are compared to the chromised specimen with no flow channel after 2000 seconds of the potentiostatic polarization test. It revealed that the substrate without milled flow channels had the best current density at about 4.6 $\times 10^{-6}$ A/cm^2; it also indicated the plating Ni and Cr pack cementation layers deposited uniform on the substrates. In the substrates after milling flow channels, the specimen milled at 100 mm/min had the best current density at about 2.3 $\times 10^{-5}$ A/cm^2; this also indicated that the feed rate at 100 mm/min was an optimal feed parameter and leaded to a smoother surface inner flow channels.

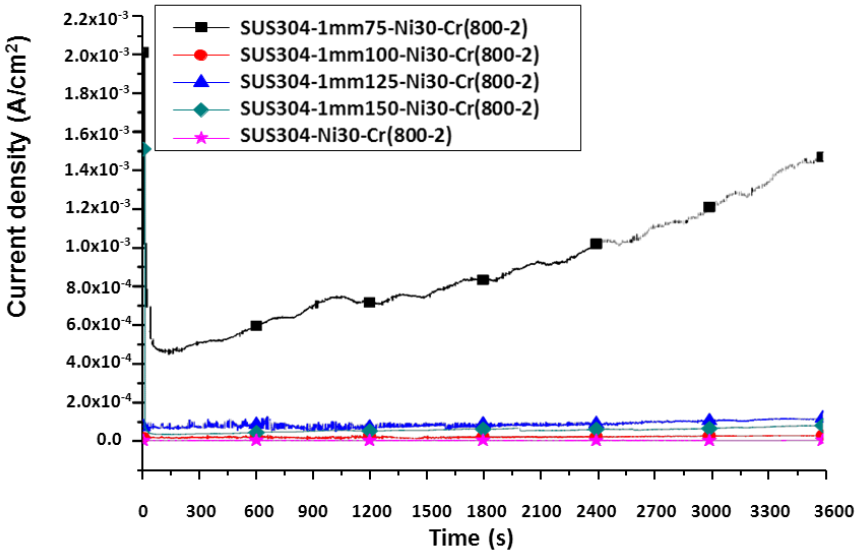

Figure 9. Static polarization curves of specimens following differential feed rate channel after pack cementation in H_2SO_4 solution at 80℃ applied 0.6 V (cathode environment).

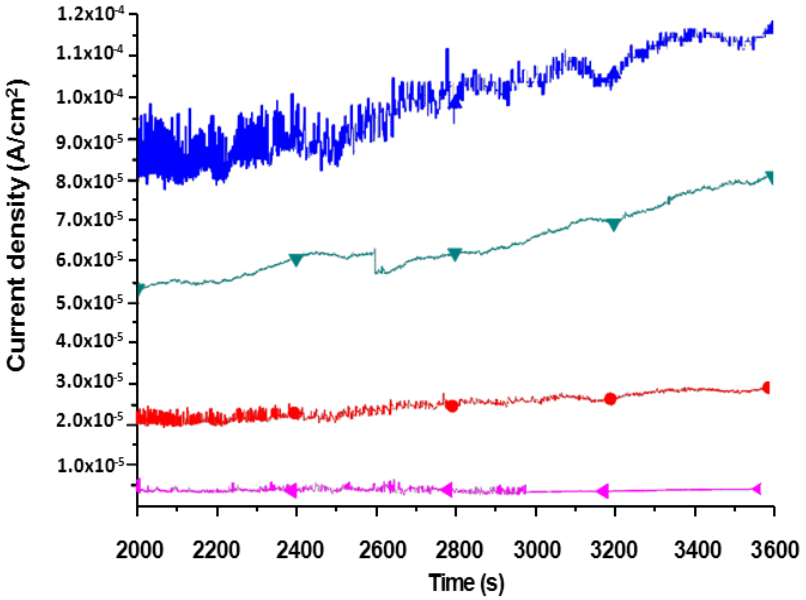

Figure 10. Local enlarge potentiostatic curves after 2000 second in Fig.9 (H_2SO_4 solution at 80℃ and applied 0.6 V in cathode environment).

3.4 Contact resistance measurement

Fig. 11 compares the contact resistance between the chromised SUS304 substrate and the chromised specimens with channels that were milled at different rotation and feed rates. The figure shows that the contact resistance decreased as the compaction forces increased, primarily because the number of contact points between the plating and carbon paper increased with the compaction force.

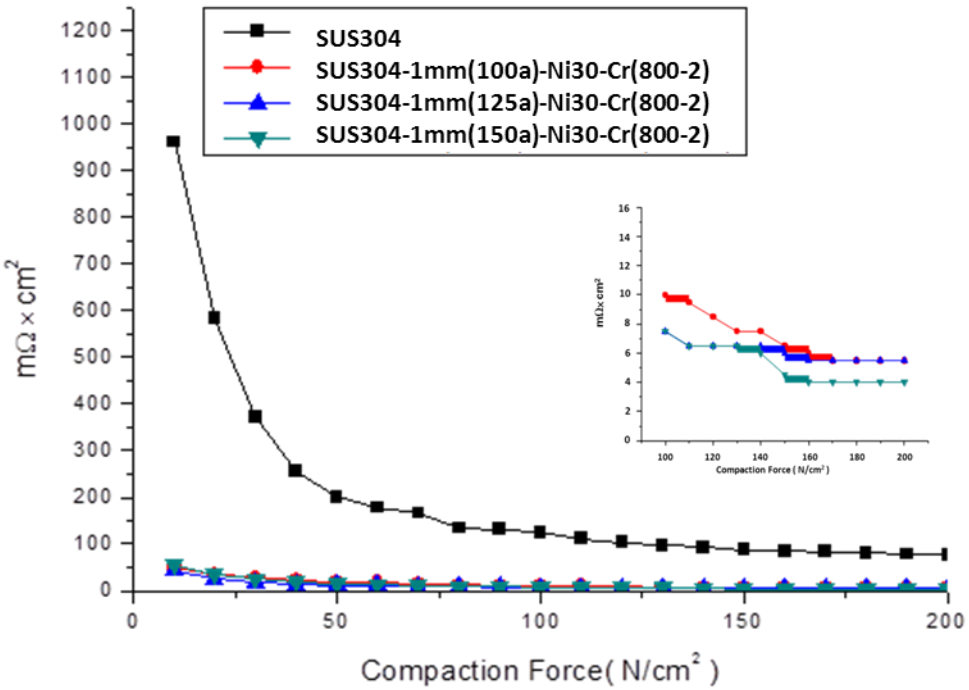

Figure 11. Variation of interfacial contact resistance between steel and carbon paper measured with clamping pressure.

4. CONCLUSIONS

SUS304 stainless steel was used as a substrate to fabricate specimens in the MC at different rotation and feed rates to simulate metal bipolar plates. The specimens were subjected to a basic pretreatment of Ni plating before being chromised (pack cementation) at 800 °C for 2 hours, which resulted in the formation of highly corrosion-resistant Cr-rich plating with low contact resistance on the surface. The following conclusions were drawn from the experimental results.

(1) The surface morphology showed that both the slow and fast feed rates produced defects inside the flow channel after pack cementation. For the slow feed rates, the overly slow movement of the cutter may have caused the temperature on the work surface to rise; thus, metal chips adhered to and fell off from the surface repeatedly, resulting in defects on the machined surface. During milling at high rotations and fast feed rates with high-pressure air cooling, the cutter moved faster and produced less tear and processing-induced stress in the material; thus, the stress could be released by pack

cementation. Cutting at slow speeds left more defects inside the channel even after pack cementation, which resulted in passivation under high currents during potentiodynamic polarization.

(2) The average corrosion current in the potentiostatic polarization test was close to the corrosion current in the potentiodynamic polarization test at 0.6 V. The initial current density of specimen SUS304-1mm100-Ni30-Cr(800-2) was no significant increase in the corrosion current of a specimen with flow channels that was remained constant from the beginning to the end of the test. Thus, this processing condition generated a better cut surface, which enabled the Cr-C coating to completely cover the cutting trace after pack cementation. The aforementioned processing parameters were found to be the optimal parameters.

(3) SUS304 stainless steel was used as a substrate for the bipolar plates of proton fuel cells and exhibited properties that were generally close to the requirements for various electrochemical tests after proper machining and the application of an anti-corrosion coating. Further studies should be performed to attain the objective of reducing the cost of bipolar plates.

References

1. S.P. Ashok, G.D. Terry, S. Nicholas, B. Elizabeth, G. Kristopher, Q. Michael, B. Christopher, *Journal of Power Sources*, 136 (2004) 220.
2. S.J. Lee, C.H. Huang, J.J. Lai, Y.P. Chen, *Journal of Power Sources*, 131 (2003) 243.
3. C.M. Robert, H.H. Arno, J. Frank, A. de Bruijn, A.M.M. Ronald K, *Fuel Cells Bulletin*, 3 (2000) 5.
4. L.X. Wang, J.C. Sun, J. Sun, Y. Lv, S. Li, S.J. Ji, Z.S. Wen, *Journal of Power Sources*, 199 (2012) 195.
5. H. Allen, C. Tapas, S Priscila, *International Journal of Hydrogen Energy*, 30 (2005) 1297.
6. H. Tawfik, Y. Hung, D. Mahajan, *Journal of Power Sources*, 163 (2007) 755.
7. S.J. Lee, C.H. Huang, Y.P. Chen, *Journal of Materials Processing Technology*, 140 (2003) 688.
8. S.H. Wang, J.C. Peng, W.B. Lui, *Journal of Power Sources*, 160 (2006) 485.
9. R.F. Silva, D. Franchi, A. Leone, L. Pilloni, A. Masci, A. Pozio, *Electrochim. Acta*, 51 (2006) 3592.
10. R.J. Tian, J.C. Sun, L. Wang, *Journal of Power Sources*, 163 (2007) 719.
11. A.E-E. Sanaa A, A.-S. Omar E, E.-A. Hammam, A. Ashraf M, *Journal of Power Sources*, 177 (2008) 131.
12. S.H. Wang, J.C. Peng, W.B. Lui, J.S. Zhang, *Journal of Power Sources*, 162 (2006) 486.
13. C.Y. Bai, T.M. Wen, K.H. Hou, M.D. Ger, *Journal of Power Sources*, 195 (2010) 779.
14. C.Y. Bai, J.L. Lee, T.M. Wen, K.H. Hou, M.S. Wu, M.D. Ger, *Applied Surface Science*, 257 (2011) 3529.
15. C.Y. Bai, T.M. Wen, K.H. Hou, N.W. Pu, M.D. Ger, *International Journal of Hydrogen Energy*, 36 (2011) 3975.
16. C.Y. Bai, M.D. Ger, M.S. Wu, *International Journal of Hydrogen Energy*, 34 (2009) 6778.
17. C.Y. Bai, M.S. Wu, M.S. Huang, K.H. Hou, M.D. Ger, S.J. Lee, *Journal of Power Sources*, 195 (2010) 5686.
18. T.M. Wen, K.H. Hou, C.Y. Bai, M.D. Ger, P.H. Chien, S.J. Lee, *Corrosion Science*, 52 (2010) 3599.
19. D. Chaliampalias, M. Papazoglou, S. Tsipas, E. Pavlidou, S. Skolianos, G. Stergioudis, G. Vourlias, *Applied Surface Science*, 256 (2010) 3618.
20. S.C. Kwon, M. Kim, S.U. Park, D.Y. Kim, K.S. Kim, Y. Choi, *Surface and Coating technology*, 183 (2004) 151.

21. C. A. Huang, W. Lin, M. J. Liao, *Corrosion Science*, 48 (2006) 460.
22. C.A. Huang, U.W. Lieu, C.H. Chuang, *Surface and Coatings Technology*, 203 (2009) 2921.
23. D.B. Lee, *Materials and Corrosion*, 59 (2008) 598.
24. C.A, Huang, C.K. Lin, W.-A. Chiou, F.-Y. Hsu, *Surface and Coatings Technology*, 26 (2011) 325.
25. Z.X. Zeng, L.P. Wang, A.M. Liang, J.Y. Zhang, *Electrochimica. Acta*, 52 (2006) 1366.
26. W.R. Chang, J.J. Hwang, F.B. Weng, S.H. Chan, *Journal of Power Sources*, 166 (2007) 149.
27. T.Y. Chiang1, A.Su., L.C. Tsai, H.B. Lee, C.Y. Lin, H.H. Sheu, C.C. Chang, *International Journal of Electrochemical Science*, 10 (2015) 1926.
28. L.C. Tsai, H.H. Sheu, C.C. Chen, M.D. Ger, *International Journal of Electrochemical Science*, 10 (2015) 317.

© 2015 The Authors. Published by ESG (www.electrochemsci.org). This article is an open access article distributed under the terms and conditions of the Creative Commons Attribution license (http://creativecommons.org/licenses/by/4.0/).